

LENSING MAGNIFICATION OF SUPERNOVAE IN THE GOODS-FIELDS

J. Jönsson, T. Dahlén, A. Goobar, and C. Gunnarsson

*Stockholm University, AlbaNova University Center,
Fysikum, SE-10691 Stockholm, Sweden*

and

E. Mörtzell

*Stockholm University, AlbaNova University Center,
Stockholm Observatory, SE-10691 Stockholm, Sweden*

and

K. Lee

*Department of Physics and Astronomy, Johns Hopkins University,
3400 North Charles Street, Baltimore, MD 21218*

jacke@physto.se

ABSTRACT

Gravitational lensing of high-redshift supernovae is potentially an important source of uncertainty when deriving cosmological parameters from the measured brightness of Type Ia supernovae, especially in deep surveys with scarce statistics. Photometric and spectroscopic measurements of foreground galaxies along the lines-of-sight of 33 supernovae discovered with the Hubble Space Telescope, both core-collapse and Type Ia, are used to model the magnification probability distributions of the sources. Modelling galaxy halos with SIS or NFW-profiles and using M/L scaling laws provided by the Faber-Jackson and Tully-Fisher relations, we find clear evidence for supernovae with lensing (de)magnification. However, the magnification distribution of the Type Ia supernovae used to determine cosmological distances matches very well the expectations for an unbiased sample, i.e. their mean magnification factor is consistent with unity. Our results show that the lensing distortions of the supernova brightness can be well understood for the GOODS sample and that correcting for this effect has a negligible impact on the derived cosmological parameters.

Subject headings: gravitational lensing – supernovae: general

1. INTRODUCTION

Having established the existence of dark energy using Type Ia supernovae (SNIa) (Riess et al. 1998; Perlmutter et al. 1999; Knop et al. 2003; Tonry et al. 2003), ongoing and planned supernova (SN) surveys are reaching sufficient sensitivity to explore the nature of the energy component of the Universe driving its accelerated expansion. One such project is the Great Observatories Origins Deep Survey (GOODS Giavalisco et al. 2004) supernova survey (Riess et al. 2004; Strolger et al. 2004), aimed at breaking the degeneracy in the cosmological parameters by expanding the redshift range of the studied SNe, as suggested by Goobar & Perlmutter (1995). However, measuring distances to $z \gtrsim 1$ SNe poses additional difficulties. The brightness dispersion caused by gravitational lensing in the inhomogeneous Universe is comparable to the intrinsic spread in SNIa luminosities. Magnification of SNe due to lensing is a systematic uncertainty that to some extent can be cured by statistics since the *mean* magnification of a large number of sources is expected to be unity relative to an homogeneous universe. However, at high redshifts where statistics are currently poor and lensing effects potentially large, magnification bias, i.e. the preferential detection of magnified sources, could affect the estimates of cosmological parameters as well as the measurements of SN rates. In order to avoid any potential bias and reduce the scatter in e.g. the Hubble diagram, it is desirable to correct the measured brightness of individual sources for their gravitational lensing. In this paper, we use a technique described in detail in an accompanying paper (Gunnarsson et al. 2005) to compute the magnification for a sample of SNe observed in the GOODS-fields, the Hubble Deep Field North (HDFN) and the Chandra Deep Field South (CDFS).

The outline of the paper is as follows. §2 contains a brief description of our method. In §3, the GOODS-fields and the SNe are presented, while we in §4 discuss systematic and statistic errors. Finally, our results are presented in §5 and discussed in §6. Throughout the paper, we use natural units, where $c = G = 1$. We use a Hubble parameter of $H_0 = 70 \text{ km s}^{-1} \text{ Mpc}^{-1}$, a matter density of $\Omega_M = 0.3$, and a dark energy density of $\Omega_\Lambda = 0.7$. If no explicit redshift dependence is shown, all quantities are given with present values. Quoted magnitudes are Vega normalized.

2. METHOD

2.1. Distribution of Matter in the Universe

The deflection and magnification of light from distant sources depend on the matter distribution in the Universe. Gravitational lensing effects are caused by inhomogeneities in

the Universe and we assume that these effects are dominated by dark matter galaxy halos.

To account for all matter in a consistent way throughout the redshift range considered in this paper ($z \lesssim 2$), all “unobserved” matter is put into a smoothly distributed component. In other words, we enforce a *global* self-consistency on our cosmological model, where the fraction of the matter density not associated with observed galaxies in the data-set is characterized by the smoothness parameter $\eta(z)$. If $\eta = 1$, all matter is smoothly distributed and conversely if $\eta = 0$, all matter is located in galaxy halos (clumps).

Since clumps and smoothly distributed matter focus light differently, the value of the η parameter affects the angular diameter distances used in computing the gravitational lens effects. This is discussed in more detail in e.g. Kayser et al. (1997).

If the evolution of the total matter density in the Universe is assumed to be known, $\rho_m(z) = \rho_m(0)(1+z)^3$, the smoothness parameter at different redshifts can be computed as

$$\eta(z) = 1 - \frac{\rho_g(z)}{\rho_m(z)}, \quad (1)$$

where $\rho_g(z)$ is the matter density in dark matter halos. Observed galaxy luminosities can be translated into halo masses using the relations presented in §2.2. The density of dark matter residing in halos can then be estimated in redshift bins by dividing the total mass of halos with the corresponding volume of the bin.

In this investigation, we use observational data obtained in the two GOODS fields, CDFS and HDFN (Giavalisco et al. (2004); Capak et al. (2004)). The magnitude limit adopted is $I \sim 24.5$. The redshift dependence of the η parameter for HDFN and CDFS is plotted in Figure 1. The smoothness parameter increases with redshift since with a fixed apparent magnitude limit, the depth in absolute magnitude becomes shallower at higher redshift and consequently, a decreasing fraction of the matter is accounted for by observed objects.

2.2. Galaxy Halos

We assume galaxy halos to be spherically symmetric and consider two different halo models: Singular Isothermal Spheres (SIS) and the profile of Navarro, Frenk, and White (NFW Navarro et al. 1997). The density profile of a SIS

$$\rho_{\text{SIS}}(r) = \frac{\sigma^2}{2\pi r^2}, \quad (2)$$

is characterized by the line-of-sight velocity dispersion σ of the galaxy. The NFW density profile,

$$\rho_{\text{NFW}}(r) = \frac{\rho_s}{(r/r_s)(1+r/r_s)^2}, \quad (3)$$

is dependent upon the scale radius r_s where approximately $\rho_{\text{NFW}} \propto r^{-2}$ and ρ_s the density at $r \sim r_s/2$. For the total mass of a halo described by any of these two profiles to be finite, the halo must be truncated at some radius r_t . We have chosen to truncate the halos at r_{200} , defined as the radius inside which the mean mass density is 200 times the present critical density. The total mass of a halo is thus m_{200} , the mass enclosed within r_{200} . For a SIS halo, m_{200} can be obtained from the velocity dispersion

$$m_{200}^{\text{SIS}} = \frac{\sqrt{2}\sigma^3}{5H_0}. \quad (4)$$

Properties of NFW halos are completely specified by m_{200} , since r_s and ρ_s can be obtained numerically from m_{200} (Navarro et al. 1997). Furthermore, we assume that $m_{200}^{\text{NFW}} = m_{200}^{\text{SIS}}$.

We estimate the velocity dispersion of each galaxy using absolute magnitudes M_B derived from observations, combined with empirical Faber-Jackson (F-J) and Tully-Fisher (T-F) relations for ellipticals and spirals, respectively. Ellipticals are defined as objects whose observed Spectral Energy Distributions (SED) are best fitted by an early type spectral template. Spirals are objects best-fitted by spiral or later type template SEDs. For ellipticals, we use the following expression for velocity dispersion derived in Mitchell et al. (2005)

$$\log_{10} \sigma = -0.091(M_B - 4.74 + 0.85z'), \quad (5)$$

where we use $z' = z$ for redshifts $z < 1$ and $z' = 1$ for $z > 1$. This redshift dependence accounts for the general brightening of the stellar population with look-back time. At high redshift ($z > 1$), where this evolution is not well known, we assume a non-evolving brightness. We let the error in the derived relation be represented by the observed scatter in the Sloan Digital Sky Survey (SDSS) measurements (Sheth et al. 2003)

$$\text{rms}(\log_{10} \sigma) = 0.079[1 + 0.17(M_B + 19.705 + 0.85z')]. \quad (6)$$

We use the T-F relation derived by Pierce & Tully (1992), with correction for redshift dependence calculated by Böhm et al. (2004), to derive the rotation velocity for the spiral/late-type population,

$$\log_{10} V_{\text{max}} = -0.134(M_B + 3.61 + 1.22z'), \quad (7)$$

where V_{max} is the maximum rotation velocity for the galaxy. The observed scatter in the absolute magnitude around this relation is $\text{rms}(M_B) = 0.41$ (Pierce & Tully 1992), corresponding to

$$\text{rms}(\log_{10} V_{\text{max}}) = 0.06. \quad (8)$$

We finally convert the rotation velocity in the spiral galaxies to a velocity dispersion using $\sigma = V_{\max}/\sqrt{2}$.

2.3. Gravitational Lensing

We follow the method developed in the accompanying paper by Gunnarsson et al. (2005) to compute magnification of SNe using a substantially modified version of a publicly available `Fortran` code, Q-LET, which utilizes the so-called multiple lens plane algorithm. The method is only briefly outlined here and we refer the reader to Gunnarsson et al. (2005) and Gunnarsson (2004) for more details.

The lens equation for multiple lens planes relates the observed and intrinsic positions of a source by tracing a light-ray through planes situated at each lens redshift upon which each lens' mass distribution is projected. From the image plane and in every consecutive plane, the deflection angle is computed and the ray is recursively followed to the source plane. Using the Jacobian determinant of the lens equation, the magnification can also be found. Whereas the deflection angle only depends on the mass within the rays impact radius on the lens (for circularly symmetric mass density projections), the magnification also depends on the surface mass density at this radius. Both quantities are therefore dependent on the mass and density profile of the lens halo. Furthermore, the distances (which depend on the η parameter) to the planes involved are important in the calculations, affecting both the deflection angle and magnification.

The magnification factor μ' obtained for a specific model universe is given relative to a universe with the same amount of smoothly distributed matter [i.e. the same smoothness parameter $\eta(z)$] but with all matter in clumps infinitely far from the line-of-sight (Dyer & Roeder 1973) implying $\mu' \geq 1$ (for primary images).

In the following, we will present our results in terms of the magnification μ relative to a universe with *all* matter distributed homogeneously ($\eta = 1$). The magnifications are related by

$$\mu = \mu' \left(\frac{D_s^{\text{fb}}}{D_s^{\eta(z)}} \right)^2, \quad (9)$$

where D_s^{fb} and $D_s^{\eta(z)}$ are angular diameter distances to the source calculated using $\eta = 1$ (or the filled-beam approximation) and $\eta(z)$, respectively (Gunnarsson et al. 2005). Due to flux conservation, the mean value of μ for random source positions is unity (Schneider et al. 1992).

3. DATA SETS

We have examined a sample of high-redshift supernovae detected within GOODS. Of the total 42 SNe detected during the survey (Riess et al. 2004; Strolger et al. 2004), we analyze 32 SNe, divided into 19 Type Ia SNe and 13 core-collapse SNe. The ten SNe that we do not include either lack a determination of, or have uncertain redshifts, or are outside the area in which we have high precision photometric redshifts for the foreground galaxies. We also include the previously detected high-redshift SN 1997ff in our sample (Riess et al. 2001).

Photometric redshifts for all foreground galaxies are calculated using photometry from the GOODS CDFS and HDFN data sets. For CDFS we include *HST* ACS *BViz* and VLT ISAAC *JHK_S* photometry (Giavalisco et al. 2004), while for the HDFN, we use KPNO-4m MOSAIC *U*-band and SUBARU 8.2m SuprimeCam *BVRIZ*-band data (Capak et al. 2004), together with KPNO-4m FLAMINGOS *JK_s*-band data obtained in March 2003. We use a version of the template fitting method to derive photometric redshifts as described in Dahlén et al. (2005). The photometric redshift code calculates for each object the best-fitting redshift, the redshift probability distribution and the best-fitting spectral type.

The accuracy of the photometric redshift code is tested by comparing with available spectroscopic redshifts. For GOODS HDFN, we use 848 spectroscopic redshifts taken from the Team Keck Treasure Redshift Survey¹ and find $\Delta_z \equiv \langle |z_{\text{phot}} - z_{\text{spec}}| / (1 + z_{\text{spec}}) \rangle \sim 0.08$ after excluding 2.4% outliers with $\Delta_z > 0.3$. For GOODS CDFS, we use 568 spectroscopic redshifts from the ESO/GOODS-CDFS spectroscopy master catalog² and find $\Delta_z \sim 0.08$ after excluding 3.7% outliers. Both the CDFS and HDFN photometric redshift catalogs are complete to $I \sim 24.5$, i.e. we are able to determine photometric redshifts for all objects to this limit. At fainter magnitudes, objects start to drop out from an increasing number of filters, making photometric redshift determination more uncertain than the quoted accuracy. Therefore, we only include objects to this limit. For objects with available spectroscopic redshifts, we replace the photometric redshifts with these.

Rest-frame absolute magnitudes and colors are derived using the recipe in Dahlén et al. (2005). In summary, the absolute magnitude in, e.g., the *B*-band, is calculated using the two observed bands that encompass the rest-frame *B*-band at the given redshift. Each observed band is K-corrected to the effective wavelength of the *B*-band using the spectral shape of the best-fitting template SED. The final magnitude is thereafter calculated by interpolating

¹http://www2.keck.hawaii.edu/realpublic/science/tksurvey/data_products/data_products.php

²http://www.eso.org/science/goods/spectroscopy/CDFS_Mastercat/

between the two magnitudes, giving more weight to the filter that observe closest to the rest-frame B -band, and subtracting the distance modulus.

4. ERROR ESTIMATION

The accuracy of our results depend on the validity of the assumption that unobserved matter can be treated as smoothly distributed and that our modeling of galaxy halos is correct. According to simulations in Gunnarsson et al. (2005) a magnitude limit of $I = 25$, approximately corresponding to the magnitude limit of the GOODS, introduce negligible errors in μ compared to these uncertainties.

The largest uncertainties involved in the modeling of galaxy halos, apart from the choice of halo model, emerge from uncertainties in galaxy redshifts and scatter in the Faber-Jackson and Tully-Fisher relations. Monte-Carlo simulations were used to obtain the errors in the estimated magnifications due to these uncertainties. New galaxy catalogs were simulated based on the GOODS-fields, where the position of each galaxy was kept fixed, but redshift and hence absolute magnitudes were varied. In the case of a photometrically measured redshift, the simulated redshift was drawn from the probability distribution of the photometric redshift. For galaxies with spectroscopic redshifts, the simulated redshift was drawn from a normal distribution with standard deviation $\sigma_z = 0.01$. Depending on the redshift probability distribution of the galaxies, foreground galaxies of a SN sometimes become background galaxies in the simulated catalogs and vice versa. The effects of galaxies popping in and out of SN lines-of-sight can be very dramatic and therefore introduce large uncertainties. When the velocity dispersion of a simulated galaxy was computed, the scatter in the Faber-Jackson and Tully-Fisher relations were taken into account. The m_{200} parameter of a galaxy is, according to equation (4), proportional to σ^3 and therefore, the scatter in the Faber-Jackson and Tully-Fisher relations, expressed by equation (6) and (8), were translated into a scatter in σ^3 , or equivalently, a scatter in m_{200} . Simulated velocity dispersions were drawn from a normal distribution of σ^3 -values with the translated scatter as standard deviation. For each simulated catalog, $\eta(z)$ was computed and any negative parts of $\eta(z)$ were set to zero. The magnification factor μ of each SN was computed for 500 simulated galaxy catalogs and the resulting Probability Distribution Functions (PDF) were used to estimate the uncertainties in the SN magnifications.

5. RESULTS FOR 33 SNE IN THE GOODS-FIELDS

Figure 2 shows the foreground galaxies within $20''$ from the four SNIa most affected by gravitational lensing in the GOODS-fields: SNe 2002fx, 2003az, 1997ff, and 2003es. Redshifts and masses of the galaxies are indicated in the figure. In Figure 3 the magnification PDFs of these SNe, computed for two different halo models, are presented. The upper and lower panels show examples of de-magnified and magnified SNe, respectively. In general, highly magnified SNe have broader PDFs than moderately magnified or de-magnified ones, since they are more model sensitive, and thus the estimated errors increase with magnification. As can be seen from Figure 2, the magnified SNe 1997ff and 2003es have more crowded lines-of-sight than the de-magnified SNe 2002fx and 2003az.

Collected results for the 20 GOODS SNIa are presented in Table 1. The table contains the magnification of the SNe and the 68% and 95% confidence intervals, computed for both SIS and NFW halo models, obtained by Monte-Carlo simulations. Included in the table are also the number of foreground galaxies within $60''$ to each SN. In Figure 4 the results are presented graphically, showing 95% confidence levels. Table 2 and Figure 5 show the same results for the 13 core-collapse SNe. We see that the difference between PDFs computed assuming SIS and NFW halos are small for most SNe but noticeable for some, like SN 2003es (see Figure 3). However, the PDFs computed for different halo models always overlap and we conclude that our method is fairly insensitive to this uncertainty. An important fact is that the SNe which we have found to be significantly magnified or de-magnified have errors smaller than the estimated magnification factor and it should thus be possible to correct for this gravitational lensing in a meaningful way.

5.1. Correlation between Redshift and Magnification

In Figure 6 the magnification, computed assuming NFW halos, of all 33 SNe is plotted vs. redshift. Type Ia and core-collapse SNe are indicated by filled circles and squares, respectively. The magnification scatter obviously increases with redshift for the two samples individually, as well as for the joint sample. Since the difference between D_s^{fb} and $D_s^{\eta(z)}$ increases with redshift, we also expect the magnification μ to be anticorrelated with redshift for lines-of-sight with few lensing galaxies where $\mu' \sim 1$, see equation (9). This trend is readily seen in Figure 6.

The scatter of magnifications expected from simulations (Gunnarsson et al. 2005) is also indicated in the figure. The most likely magnification as a function of redshift is indicated by the dashed line. Light and dark gray shaded areas represent the 68% and 95% confidence

level of the simulated distributions, respectively. The magnification of GOODS supernovae follow the redshift trend expected from simulations and the scatter is in agreement with the simulated data. We can thus not find any evidence for any unexpected magnification bias with redshift.

5.2. Distributions of Magnifications

The distribution of magnifications (for the NFW case) of our GOODS SNe is shown in Figure 7, a histogram based on the joint sample of both Type Ia and core-collapse SNe. The distribution peaks at a value slightly lower than unity and has a tail toward large magnifications. Moreover, the mean of the distribution is close to unity. Since the field size is finite, implying that not *all* lenses are included, and the fact that any multiple images are left out, we *do* expect the mean value of the magnification to be slightly lower than unity (see also Gunnarsson et al. 2005). The figure also shows, in shaded gray, the expected distribution of magnifications for our sample of SNe obtained by simulations. Although the SN sample is small, the agreement between GOODS SNe and simulated data is excellent.

We have also compared the distribution of the magnification of $\sim 9\,000$ randomly picked source positions at $z = 1.5$ in the GOODS-fields to a distribution simulated with the SNOC package (Goobar et al. 2002) used previously to estimate SN lensing uncertainty in e.g. Knop et al. (2003). The distributions, computed assuming NFW halos, are presented in Figure 8, where we see that the difference between the distributions for CDFS and HDFN is very small and that the mean value of the distributions are again slightly less than unity. The agreement between the distributions for the GOODS-fields and the simulated distribution is fairly good although the simulated distribution, which does not include any large scale structure effects, peaks at a slightly higher value than the one for the GOODS-fields. We conclude that the distribution of magnifications obtained using the SNOC package is comparable to a real distribution and hence realistic.

5.3. The Magnification of SN 1997ff

The issue of magnification of the farthest known SN, SN 1997ff, has been addressed by several authors in the past (Lewis & Ibata 2001; Riess et al. 2001; Mörtzell et al. 2001; Benítez et al. 2002). In the analysis of Lewis & Ibata (2001) two galaxies very close to the line-of-sight were considered, both residing at $z = 0.56$ and visible in Figure 2. Lewis and Ibata assumed both galaxies to have the same velocity dispersion and calculated the magnification

for three different values. For velocity dispersions 100 km s^{-1} , 200 km s^{-1} , and 300 km s^{-1} they found a magnification of -0.084 mag , -0.38 mag , and -1.16 mag , respectively. The velocity dispersions of these galaxies are closer to 100 km s^{-1} than 200 km s^{-1} and the most likely magnification estimated by Lewis and Ibata is consequently -0.084 mag . Lensing by one of these two galaxies was also studied in Riess et al. (2001) concluding a low probability for any significant lensing. More foreground galaxies were considered in the estimation of the magnification of SN 1997ff by Mörtzell et al. (2001), who considered galaxies within $10''$ from the SN. However, due to uncertainties in the Faber-Jackson relation normalization they found the range of magnifications to be too large to allow any quantitative statement. Benítez et al. (2002) included 6 galaxies within $15''$ in their analysis and reported a magnification of $\sim -0.3 \text{ mag}$, although overestimating the velocity dispersions. In their re-analysis the magnification is significantly reduced (Benítez, N., private communication). However, the above-mentioned estimates all use the filled-beam approximation for calculating distances, i.e. the lensing galaxies are put on top of a universe with all matter distributed homogeneously. Since in this approach, every line-of-sight is overdense compared to a homogeneous universe, $\mu \geq 1$ (if the image is primary) and magnifications are overestimated.

Including galaxies within $60''$ and using SIS and NFW halo models, we find a magnification of $-0.13_{-0.02}^{+0.07} \text{ mag}$ and $-0.18_{-0.02}^{+0.08} \text{ mag}$ (68% confidence levels) relative to an homogeneous universe, respectively.

5.4. Cosmology Fits

We have computed corrections for 14 of the 157 “gold” SNe in Riess et al. (2004). In this section the implications on cosmology fits due to these corrections are investigated. The magnitude of SN 1997ff published in Riess et al. (2004) has been corrected for gravitational lensing (Riess, A., private communication) and to facilitate comparisons of fits of cosmological parameters with and without corrections for gravitational lensing we have subtracted 0.34 mag (Benítez et al. 2002) from the magnitude of SN 1997ff.

Figure 9 show the results of fits of Ω_M and Ω_Λ to the data in the top panel. In the bottom panel the results of fits of Ω_M and a constant dark energy equation of state w_0 to the data, assuming a flat universe, are presented. Contours are given at 68%, 95%, and 99% confidence levels.

The confidence level contours of the corrected fit in the top panel move $\sim 4\%$ along the major axis of the confidence level ellipses toward smaller values relative to the uncorrected fit. The effects of the corrections are small also on the Ω_M and w_0 fit. In both cases, fits to

the corrected data are in better agreement with the concordance model than the uncorrected data. Noting that the difference between fits to the corrected and uncorrected data is small, one should bear in mind that corrections have been applied only to 14 out of the 157 SNe and the effects could thus potentially be larger. No uncertainties in the corrections have been taken into account in the fits. Neglecting possible selection effects, simulations of the entire “gold” sample indicate that the added uncertainty due to lensing on the estimates of dark energy is $\sigma_{\Omega_\Lambda} \approx 0.04$. Assuming a flat universe, the lensing uncertainty on the equation of state parameter becomes $\sigma_{w_0} \approx 0.09$.

6. SUMMARY AND DISCUSSION

In Gunnarsson et al. (2005) a technique for correcting observed magnitudes of point sources for magnification by gravitational lensing was presented and it was also shown that the scatter due to gravitational lensing can be reduced by this technique. The technique has been applied to the published sample of Hubble Space Telescope discovered SNe in the GOODS-fields (Riess et al. 2004; Strolger et al. 2004). Our study shows clear evidence for magnified and de-magnified SNe. We show explicitly that it is possible to correct for gravitational lensing of SNe, thereby decreasing some of the induced smearing in the Hubble diagram at high redshift. We find that the mean magnification factor for the 33 SNe in the GOODS-fields is very close to unity, i.e. we find no signs of magnification selection effects on the sample. The scatter is consistent with the results of simulations in e.g. Goobar et al. (2002). For the most magnified supernova, SN 1997ff, we find a magnification below -0.25 mag with 95% confidence level, i.e. smaller than what previous studies of this SN concluded.

The effect of the corrections due to gravitational lensing on the current cosmology fits is small. We have computed the corrections for 14 of the gold SNe in Riess et al. (2004). If the corrected magnitudes for these SNe are used and Ω_M and Ω_Λ fitted to the gold sample, confidence contours move $\sim 4\%$ along the major axis of the confidence level ellipses toward smaller values.

Since magnified SNe appear brighter, we expect a correlation between the residual magnitudes in the Hubble diagram after subtracting the best-fit cosmology magnitudes and the lensing magnification factor. Rank correlation tests for the Type Ia SNe for which we have estimated the magnification factor, μ , show a correlation between μ and the residual magnitudes of the expected order. However, uncertainties in both μ and the observed magnitudes are large and they can be described as having zero correlation within the 68% confidence level.

Although our method takes into account undetected matter, there are a few caveats concerning the distribution of matter. If light does not trace matter, the distribution could be different from what we have inferred from the observed galaxies. The center of dark matter halos could be different from the center of galaxies. Moreover, the existence of dark halos or even dark compact objects not associated with galaxies is unlikely, but cannot be excluded at the moment. Similarly, we have neglected the possible non-spherical shapes of dark matter halos. However, the small differences in the magnification probabilities we found between the NFW and SIS halo profiles, along with tests we have done indicating that $0.5''$ offsets in the positions of the lenses have also negligible impact in the results presented here indicate that the technique is robust. Thus, we conclude that correcting for gravitational lensing is advantageous when using standard candles to determine cosmological distances.

The authors would like to thank Joakim Edsjö, Daniel Holz, Saul Perlmutter and Jesper Sollerman for helpful discussions during the course of the work. AG is a Royal Swedish Academy Research Fellow supported by grants from the Swedish Research Council, the Knut and Alice Wallenberg Foundation and the Göran Gustafsson Foundation for Research in Natural Sciences and Medicine. CG would like to thank the Swedish Research Council for financial support.

REFERENCES

- Benítez, N., Riess, A., Nugent, P., Dickinson, M., Chornock, R., & Filippenko, A. 2002, *ApJ*, 577, L1
- Böhm, A., et al. 2004, *A&A*, 420, 97
- Capak, P., et al. 2004, *AJ*, 127, 180
- Dahlén, T., Mobasher, B., Somerville, R., Moustakas, L., Dickinson, M., Ferguson, H., Giavalisco, M. 2005, *ApJ*, 631, 126
- Dyer, C. & Roeder, R. 1973, *ApJ*, 180, 31
- Giavalisco, M., et al. 2004, *ApJ*, 600, L93
- Goobar, A., Perlmutter, S. 1995, *ApJ*, 450, 14
- Goobar, A., Mörtzell, E., Amanullah, R., Goliath, M., Bergström, L., Dahlén, T. 2002, *A&A*, 392, 757

- Gunnarsson, C., Dahlén, T., Goobar, A., Jönsson, J., & Mörtzell, E. 2005, ApJ, submitted
- Gunnarsson, C., 2004, JCAP, 0403, 002
- Kayser, R., Helbig, P., Schramm, T. 1997, A&A, 318, 680
- Knop, R., et al. 2003, ApJ, 598, 102
- Lewis, G., & Ibata, R. 2001, MNRAS, 324, L25
- Mitchell, J., Keeton, C., Frieman, J., Sheth, R. 2005, ApJ, 622, 81
- Mörtzell, E., Gunnarsson, C., & Goobar, A., 2001, ApJ, 561, 106
- Navarro, J., Frenk, C., & White, S. 1997, ApJ, 490, 93
- Perlmutter, S., et al. 1999, ApJ, 517, 565
- Pierce, M., & Tully, R. 1992, ApJ, 387, 47
- Riess, A., et al. 1998, AJ, 116, 1009
- Riess, A., et al. 2001, ApJ, 560, 49
- Riess, A., et al. 2004, ApJ, 607, 665
- Schneider, P., Ehlers, J., Falco, E. 1992, Gravitational Lenses (Berlin: Springer-Verlag)
- Sheth, R., et al. 2003, ApJ, 594, 225
- Strolger, L., et al. 2004, ApJ, 613, 200
- Tonry, J., et al. 2003, ApJ, 594, 1

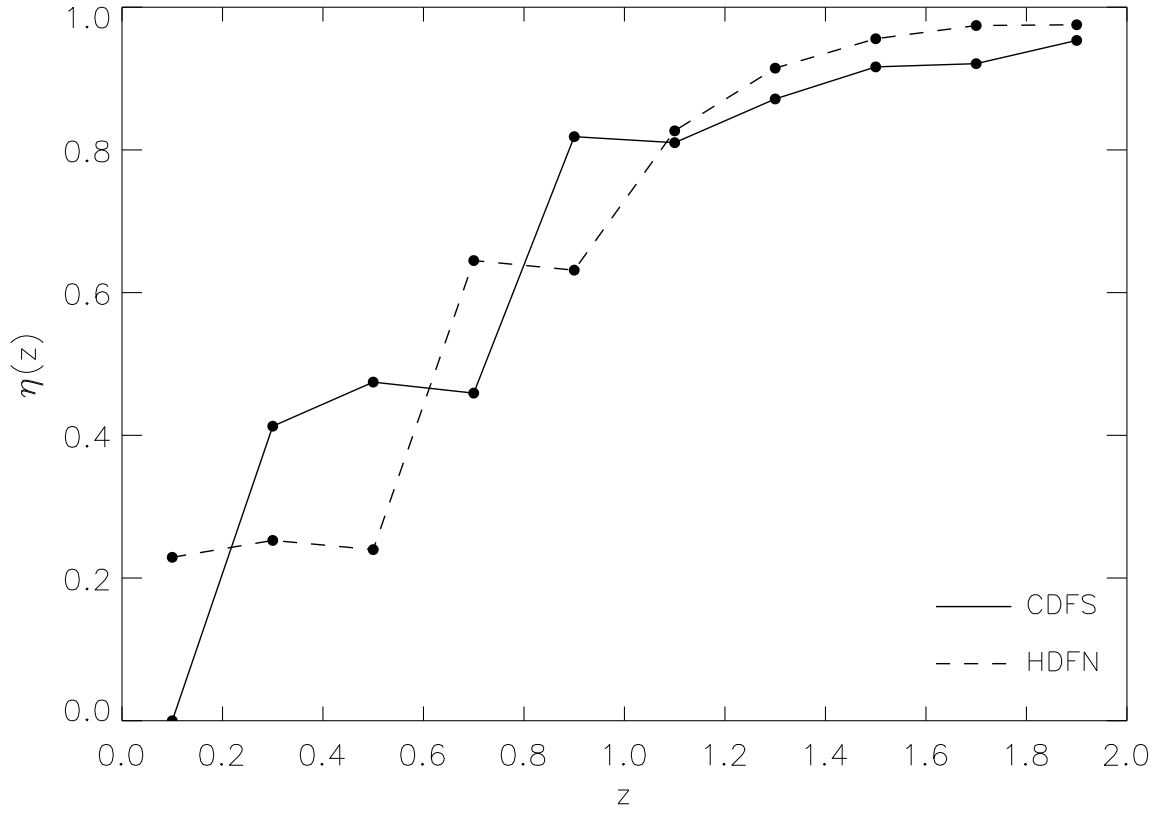


Fig. 1.— Redshift dependence of the smoothness parameter. The solid and dashed line show $\eta(z)$ vs. redshift computed for the CDFS- and HDFN-field, respectively.

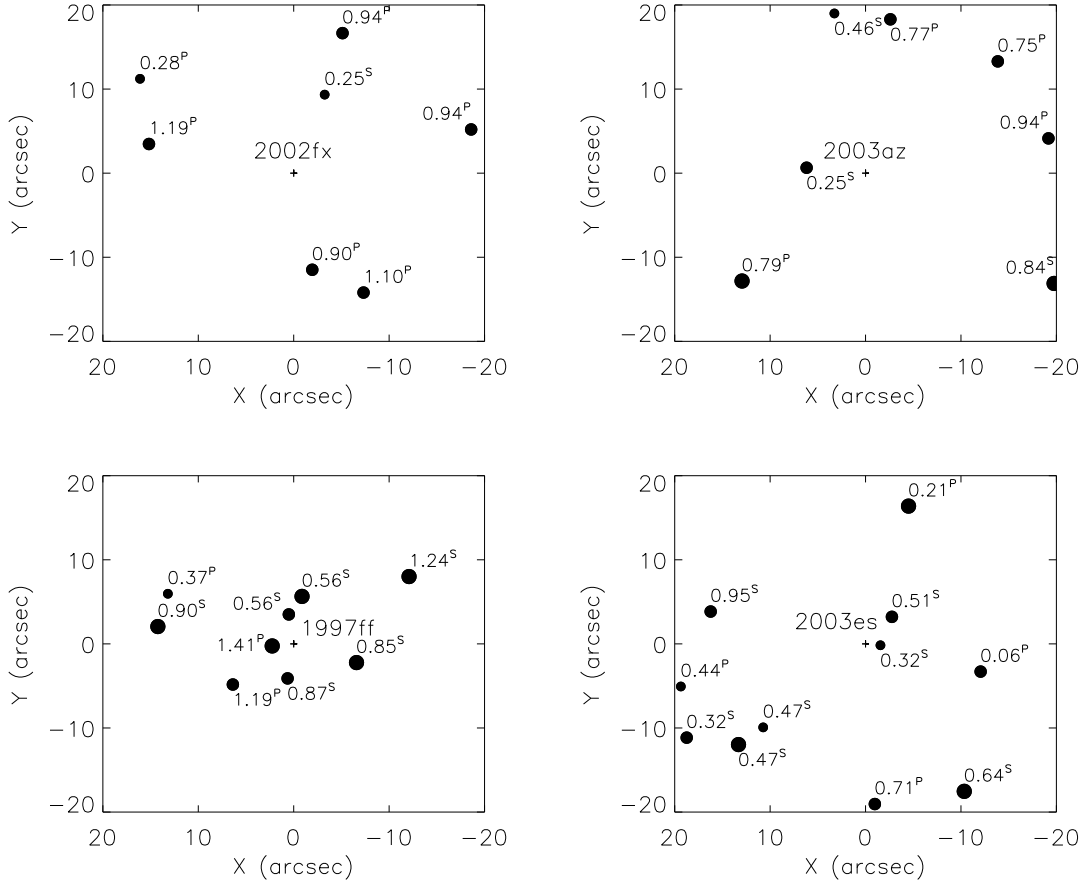


Fig. 2.— Lines-of-sight to four of the supernovae most affected by lensing. The SN is indicated by a cross at (0,0). Masses of foreground galaxies are proportional to the size of the plot symbols. Small, medium sized, and large filled circles indicate foreground galaxies with masses $m_{200}/M_{\odot} \leq 10^{11}$, $10^{11} < m_{200}/M_{\odot} < 10^{12}$, and $m_{200}/M_{\odot} \geq 10^{12}$, respectively. Redshifts of the galaxies are written next to the galaxies and the superscripts indicate whether the redshift is spectroscopic (S) or photometric (P).

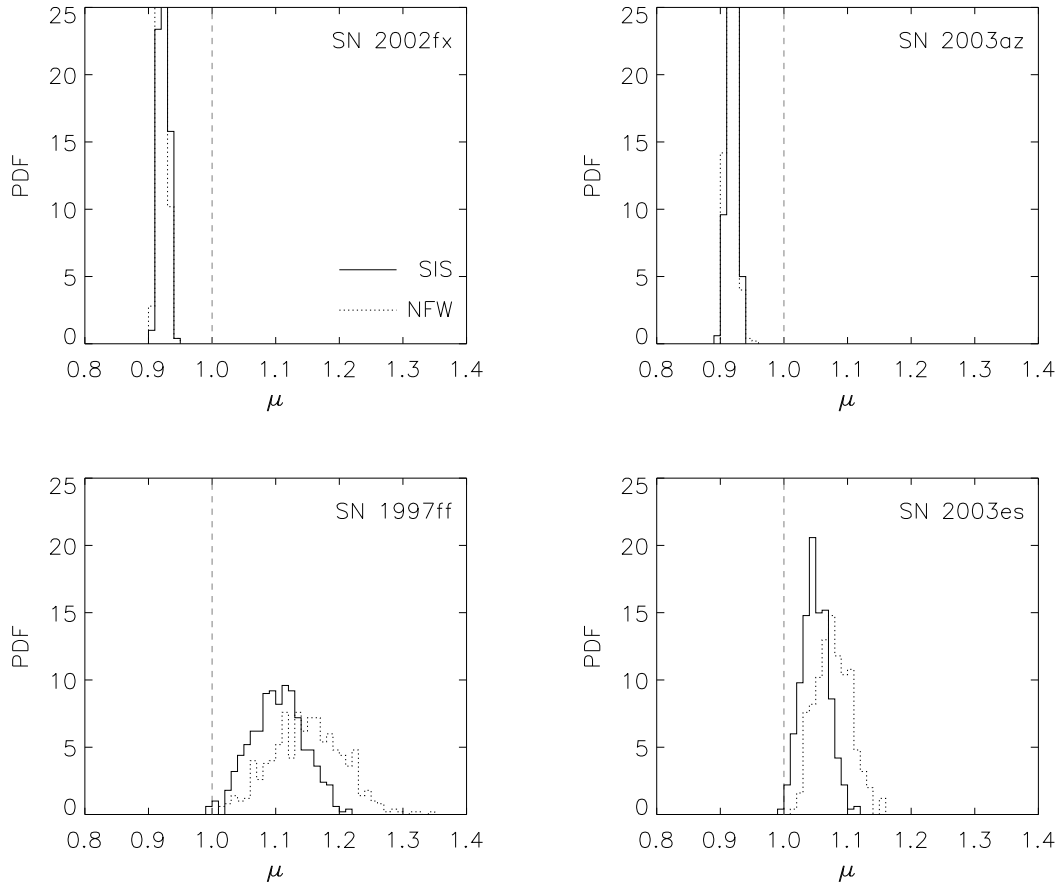


Fig. 3.— Magnification PDFs of four of the supernovae most affected by lensing. Solid and dotted lines show PDFs computed assuming SIS and NFW halo profiles, respectively.

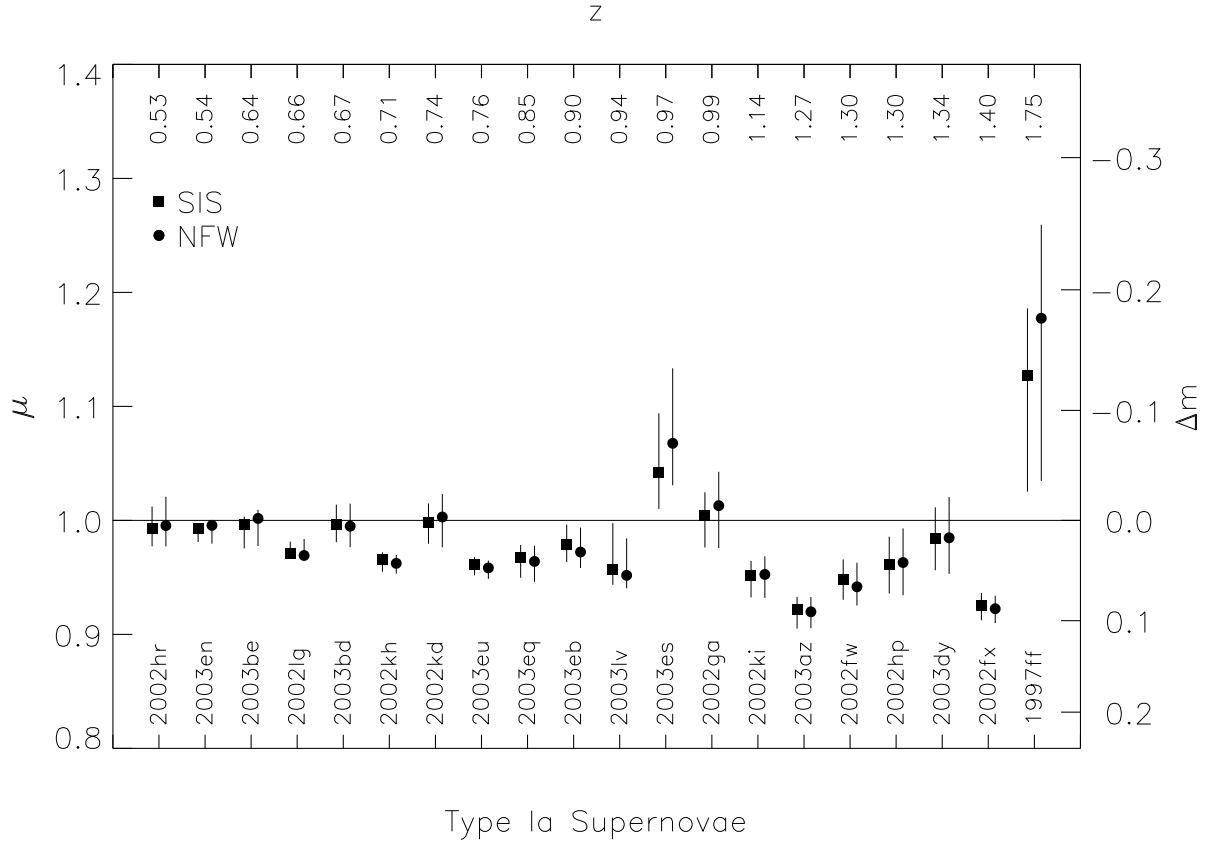


Fig. 4.— Magnification of Type Ia SNe in the GOODS-fields. Solid squares and circles indicate magnifications computed assuming SIS or NFW halo profiles, respectively. The error-bars show the 95% confidence level.

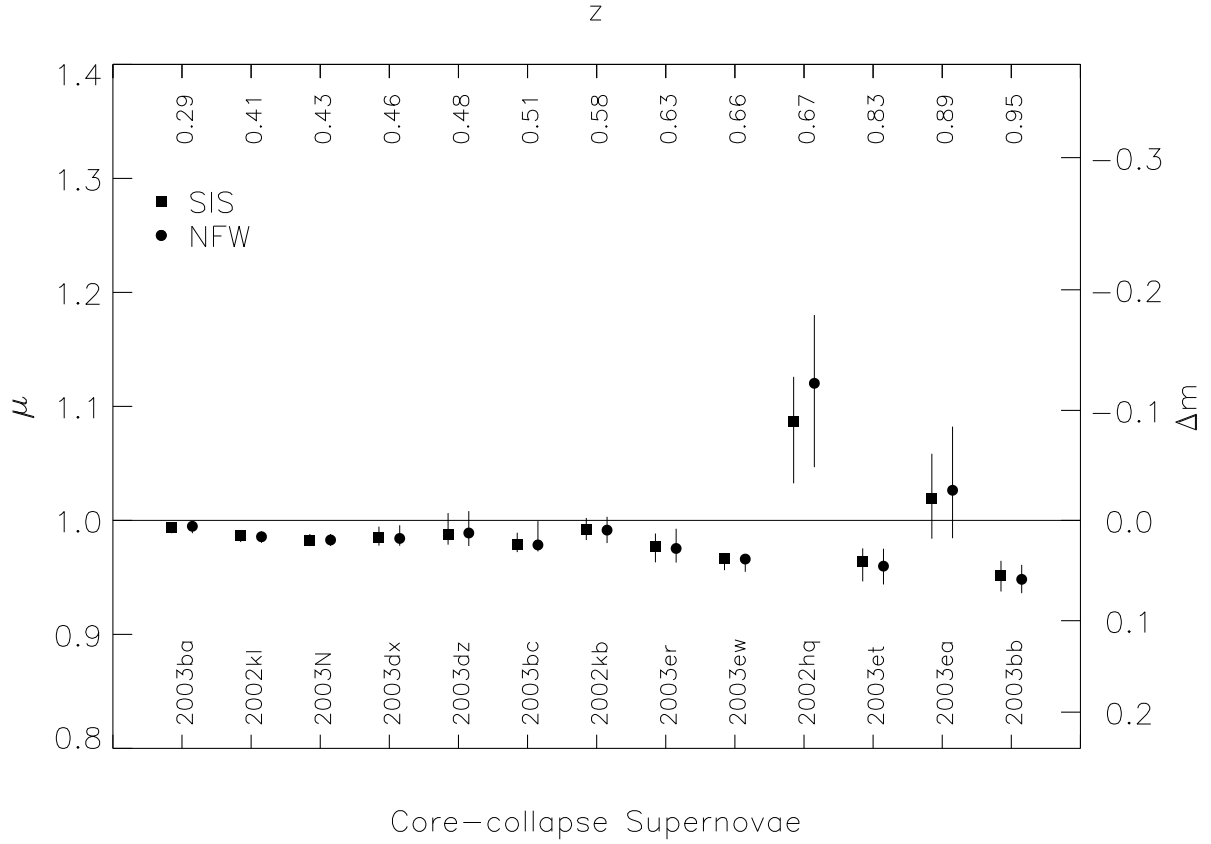


Fig. 5.— Magnification of core-collapse SNe in the GOODS-fields. Solid squares and circles indicate magnifications computed assuming SIS or NFW halo profiles, respectively. The error-bars show the 95% confidence level.

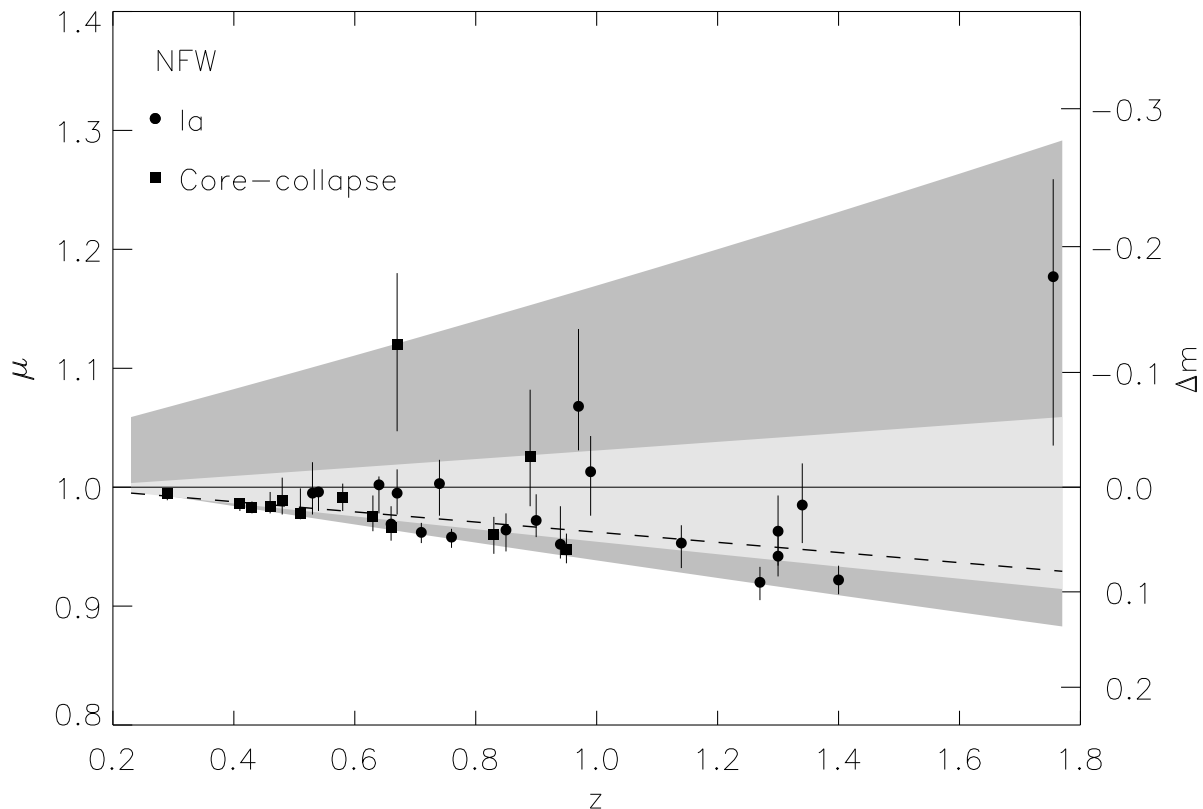


Fig. 6.— Magnification of the 33 SNe vs. redshift. Filled circles and squares represents Type Ia and core-collapse SNe, respectively. Error-bars show the 95% confidence level. The figure also shows simulated distributions of magnifications as a function of redshift at 68% (light gray) and 95% (dark gray) confidence level (Gunnarsson et al. 2005). The dashed line indicate the most probable simulated magnifications.

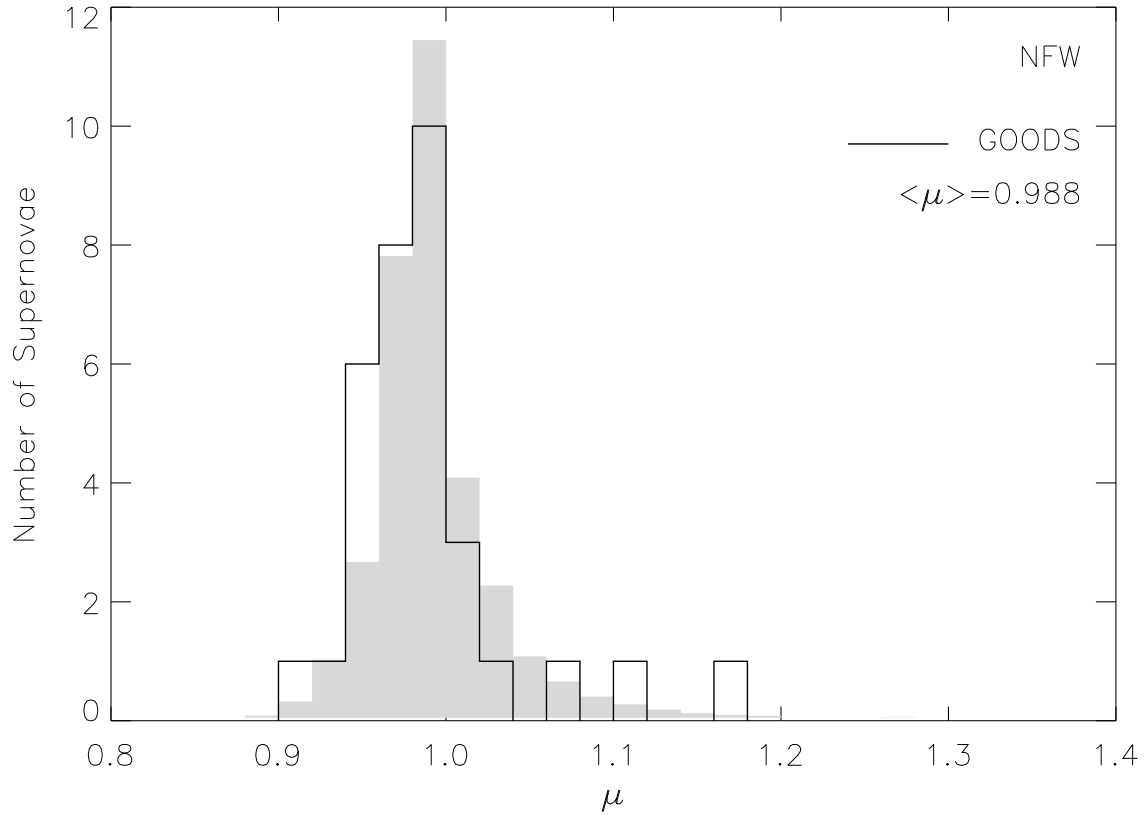


Fig. 7.— Histogram of the magnification of 33 SN in the GOODS-fields. The shaded histogram show the expected (normalized) distribution of SN magnifications from simulations.

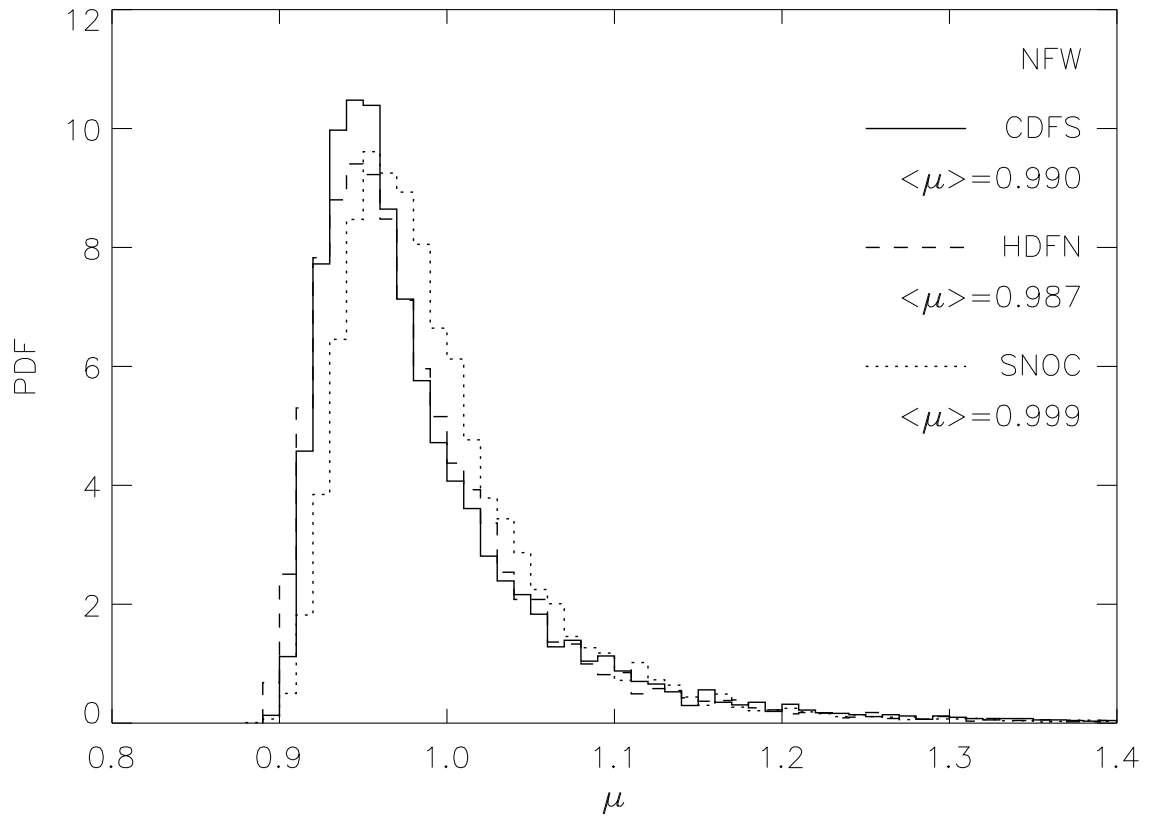


Fig. 8.— Comparison between distributions for the GOODS-fields and a simulated distribution. Solid and dashed lines indicate the distributions of magnifications obtained for $\sim 9,000$ randomly picked sources, at $z = 1.5$, in CDFS- and HDFN-field, respectively. The simulated distribution, indicated by the dotted line, was obtained using the SNOC package.

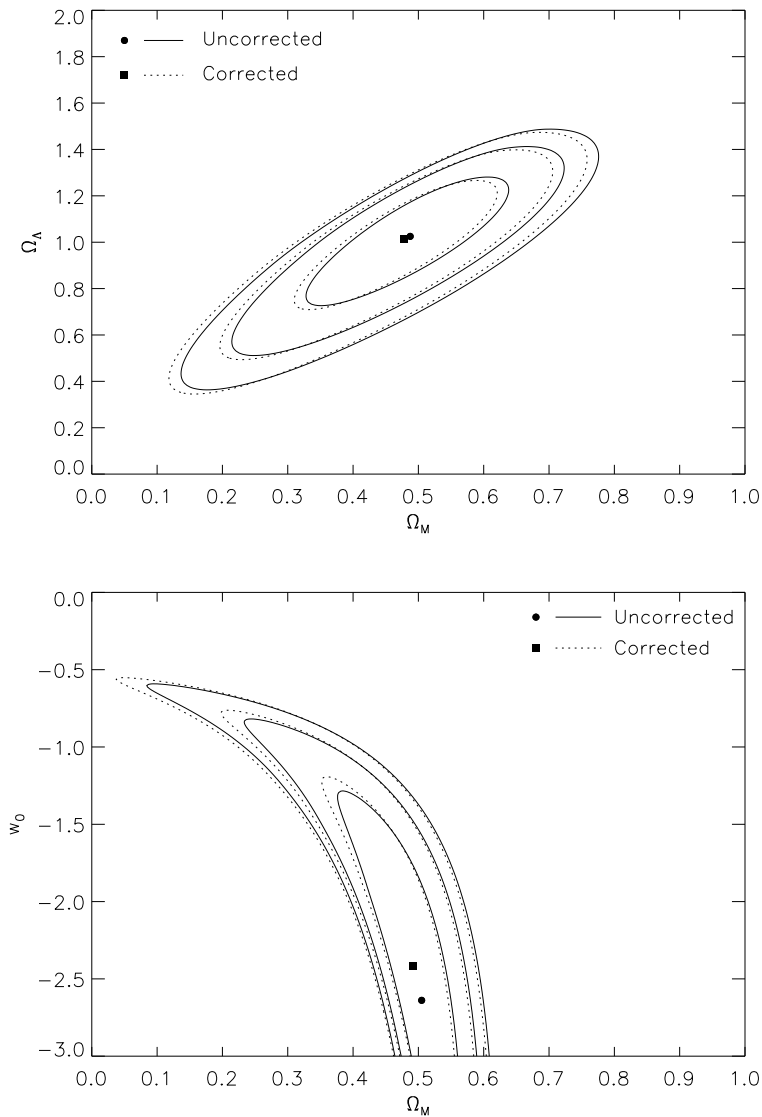


Fig. 9.— Cosmological parameter fits to “gold” SNe in Riess et al. (2004) with and without corrections for gravitational lensing. The figure shows fits of Ω_M and Ω_Λ in the top panel and of Ω_M and a constant dark energy equation of state w_0 in the bottom panel. Contours at 68%, 95%, and 99% confidence level obtained from uncorrected and corrected data are indicated by solid and dotted lines, respectively and the best fits are indicated by solid circles and squares. Note that corrections have been applied to only 14 out of 157 SNe.

Table 1. Results for Type Ia supernovae.

SN	z	N_{gal}	SIS			NFW		
			μ	68% c.l.	95% c.l.	μ	68% c.l.	95% c.l.
2002hr	0.526	14	0.993	[0.983,1.000]	[0.977,1.012]	0.995	[0.984,1.007]	[0.977,1.021]
2003en	0.54	22	0.993	[0.985,0.992]	[0.981,0.997]	0.996	[0.986,0.995]	[0.980,1.000]
2003be	0.64	26	0.996	[0.981,0.997]	[0.975,1.003]	1.002	[0.983,1.002]	[0.978,1.009]
2002lg	0.66	21	0.971	[0.970,0.977]	[0.967,0.981]	0.969	[0.969,0.977]	[0.966,0.984]
2003bd	0.67	36	0.997	[0.988,1.004]	[0.981,1.014]	0.995	[0.985,1.004]	[0.977,1.015]
2002kh	0.71	33	0.966	[0.959,0.967]	[0.955,0.972]	0.962	[0.957,0.964]	[0.953,0.970]
2002kd	0.735	47	0.998	[0.989,1.006]	[0.979,1.015]	1.003	[0.990,1.014]	[0.976,1.023]
2003eu	0.76	54	0.962	[0.955,0.964]	[0.952,0.968]	0.958	[0.952,0.960]	[0.949,0.965]
2003eq	0.839	55	0.968	[0.957,0.972]	[0.950,0.978]	0.964	[0.953,0.968]	[0.946,0.978]
2003eb	0.899	55	0.979	[0.970,0.987]	[0.963,0.996]	0.972	[0.965,0.984]	[0.958,0.994]
2003lv	0.935	48	0.957	[0.949,0.963]	[0.943,0.998]	0.952	[0.945,0.958]	[0.940,0.984]
2003es	0.97	64	1.042	[1.028,1.070]	[1.010,1.094]	1.068	[1.049,1.106]	[1.031,1.133]
2002ga	0.99	49	1.004	[0.988,1.012]	[0.976,1.025]	1.013	[0.991,1.026]	[0.976,1.043]
2002ki	1.141	52	0.952	[0.939,0.956]	[0.932,0.964]	0.953	[0.941,0.960]	[0.932,0.968]
2003az	1.27	43	0.921	[0.912,0.925]	[0.905,0.933]	0.920	[0.910,0.924]	[0.905,0.933]
2002fw	1.30	87	0.948	[0.939,0.955]	[0.930,0.966]	0.942	[0.932,0.953]	[0.925,0.963]
2002hp	1.305	65	0.962	[0.947,0.972]	[0.936,0.986]	0.963	[0.945,0.978]	[0.934,0.993]
2003dy	1.34	70	0.984	[0.971,0.999]	[0.956,1.011]	0.985	[0.969,1.001]	[0.953,1.020]
2002fx	1.40	63	0.926	[0.918,0.930]	[0.912,0.936]	0.922	[0.915,0.928]	[0.910,0.934]
1997ff	1.755	93	1.127	[1.059,1.146]	[1.025,1.186]	1.177	[1.091,1.207]	[1.035,1.259]

Table 2. Results for core-collapse supernovae.

SN	z	N_{gal}	SIS			NFW		
			μ	68% c.l.	95% c.l.	μ	68% c.l.	95% c.l.
2003ba	0.29	4	0.994	[0.990,0.994]	[0.989,0.997]	0.995	[0.990,0.995]	[0.989,0.998]
2002kl	0.41	14	0.986	[0.983,0.988]	[0.981,0.991]	0.986	[0.982,0.987]	[0.980,0.990]
2003N	0.43	16	0.983	[0.979,0.984]	[0.977,0.988]	0.983	[0.979,0.984]	[0.978,0.988]
2003dx	0.46	17	0.985	[0.981,0.989]	[0.978,0.995]	0.984	[0.981,0.990]	[0.978,0.996]
2003dz	0.48	19	0.987	[0.981,0.992]	[0.979,1.006]	0.989	[0.981,0.994]	[0.977,1.008]
2003bc	0.51	19	0.979	[0.976,0.983]	[0.972,0.989]	0.978	[0.975,0.984]	[0.973,0.999]
2002kb	0.58	27	0.992	[0.987,0.996]	[0.983,1.002]	0.991	[0.986,0.997]	[0.980,1.003]
2003er	0.63	26	0.977	[0.969,0.980]	[0.963,0.988]	0.975	[0.967,0.980]	[0.963,0.993]
2003ew	0.66	28	0.967	[0.960,0.967]	[0.956,0.971]	0.966	[0.958,0.965]	[0.955,0.970]
2002hq	0.67	27	1.087	[1.059,1.107]	[1.033,1.126]	1.120	[1.080,1.151]	[1.047,1.180]
2003et	0.83	34	0.964	[0.953,0.969]	[0.946,0.975]	0.960	[0.950,0.967]	[0.944,0.975]
2003ea	0.89	48	1.019	[1.001,1.043]	[0.984,1.058]	1.026	[1.003,1.059]	[0.984,1.082]
2003bb	0.95	52	0.952	[0.944,0.957]	[0.938,0.965]	0.948	[0.941,0.954]	[0.936,0.961]